

# Gulf Stream Excursions and Sectional Detachments Generate the Decadal Pulses in the Atlantic Multidecadal Oscillation

SUMANT NIGAM<sup>a</sup> AND ALFREDO RUIZ-BARRADAS

*Department of Atmospheric and Oceanic Science, University of Maryland, College Park, College Park, Maryland*

LÉON CHAFIK

*Geophysical Institute, University of Bergen, and Bjerknes Centre for Climate Research, 5020 Bergen, Norway*

(Manuscript received 6 January 2017, in final form 7 January 2018)

## ABSTRACT

Decadal pulses within the lower-frequency Atlantic multidecadal oscillation (AMO) are a prominent but underappreciated AMO feature, representing decadal variability of the subpolar gyre (e.g., the Great Salinity Anomaly of the 1970s) and wielding notable influence on the hydroclimate of the African and American continents. Here clues are sought into their origin in the spatiotemporal development of the Gulf Stream's (GS) meridional excursions and sectional detachments apparent in the 1954–2012 record of ocean surface and subsurface salinity and temperature observations.

The GS excursions are tracked via meridional displacement of the 15°C isotherm at 200-m depth—the GS index—whereas the AMO's decadal pulses are targeted through the AMO *tendency*, which implicitly highlights the shorter time scales of the AMO index. The GS's northward shift is shown to be preceded by the positive phase of the low-frequency North Atlantic Oscillation (LF-NAO) and followed by a positive AMO tendency by 1.25 and 2.5 years, respectively. The temporal phasing is such that the GS's northward shift is nearly concurrent with the AMO's cold decadal phase (cold, fresh subpolar gyre). Ocean–atmosphere processes that can initiate phase reversal of the gyre state are discussed, starting with the reversal of the LF-NAO, leading to a mechanistic hypothesis for decadal fluctuations of the subpolar gyre.

According to the hypothesis, the fluctuation time scale is set by the self-feedback of the LF-NAO from its influence on SSTs in the seas around Greenland, and by the cross-basin transit of the GS's detached eastern section; the latter is produced by the southward intrusion of subpolar water through the Newfoundland basin, just prior to the GS's northward shift in the western basin.

## 1. Introduction

The Gulf Stream system, which includes the Gulf Stream (GS) and its northeastward extensions, the North Atlantic and Azores Currents, is an essential component of the climate system as it transports heat and salinity from the tropics into the middle and higher latitudes. The GS system is influenced by subtropical and subpolar gyre variability (Joyce et al. 2000; Chafik et al. 2016), to which it also contributes. The leading modes of variability in the North Atlantic sector consists of an atmospheric mode

with a characteristic meridional dipole structure in sea level pressure, the North Atlantic Oscillation (NAO; Hurrell 1995; Marshall et al. 2001), and an oceanic mode with a distinctive SST pattern, the Atlantic multidecadal oscillation (AMO; Enfield et al. 2001; Guan and Nigam 2009; Kavvada et al. 2013). The former represents atmospheric variability on subseasonal-to-decadal time scales (e.g., Marshall et al. 2001; Nigam 2003) while the latter represents low-frequency SST variability, with striking decadal pulses (e.g., the Great Salinity Anomaly of the 1970s; Slonosky et al. 1997) embedded in a multidecadal oscillation (Fig. 1 herein; see also Guan and Nigam 2009).

The origin of multidecadal variability in North Atlantic SSTs (e.g., the AMO) is being actively debated. The role of oceanic processes, especially heat transports through modulation of the Atlantic meridional overturning circulation (AMOC)—a long-standing mechanism (Delworth

---

<sup>a</sup> Additional affiliation: Jefferson Science Fellow, The National Academy of Sciences, Engineering and Medicine, Washington, DC.

---

Corresponding author: Sumant Nigam, nigam@umd.edu

et al. 1993; Knight et al. 2005; Latif and Keenlyside 2011; McCarthy et al. 2015)—was recently challenged by analyses positing a role for the atmosphere via modulation of surface fluxes, specifically aerosol-influenced radiative fluxes (e.g., Booth et al. 2012) and stochastic heat flux variations (Clement et al. 2015). Rejoinders from Zhang et al. (2013, 2016), Zhang (2017), O'Reilly et al. (2016), and Drews and Greatbatch (2016) underscore the role of ocean circulation in generating multidecadal variability, suggesting that the AMO's origin is far from settled. While insightful, this debate on the AMO's origin concerns the generation of SST variability on *multidecadal* time scales and, as such, does not detract from the present study, which targets the AMO's *decadal* time scale component.

The decadal pulses embedded in the AMO are more than just intriguing: they exert strong influence on the hydroclimate of adjacent continents and on regional extreme weather. The AMO pulses have been linked to multiyear drought and wet episodes over the Great Plains in the twentieth century (including the 1930s "Dust Bowl" drought), with a correlation of approximately  $-0.7$  (Fig. 2b in Nigam et al. 2011); to decadal fluctuations in Sahel rainfall (Nigam and Ruiz-Barradas 2016); and to the decadal variations in Atlantic tropical cyclone counts (Nigam and Guan 2011). The AMO's decadal pulses are thus fascinating, with respect to both their origin and influence mechanisms.

A key goal of this analysis is to investigate the origin of decadal pulses manifest in the AMO, especially the potential role of the NAO and GS variability in their origin. Subsequent references to the NAO, as such, implicitly refer to its low-frequency component (LF-NAO) whereas those to the AMO refer to its high-frequency component, that is, to the decadal pulses apparent in the less smoothed versions of the AMO index (Fig. 1). The GS variability, in the form of meridional shifts of its north wall, is intrinsically on decadal time scales (cf. Fig. 1). It has been associated with the NAO (Taylor and Stephens 1998; Joyce et al. 2000; Frankignoul et al. 2001; de Coëtlogon et al. 2006; Kavvada 2014), with the northward shift linked to a colder, stronger subpolar gyre (Zhang 2008; Joyce and Zhang 2010). The GS's relationship with the AMO's decadal pulses has, however, not been investigated, notwithstanding its link with the subpolar gyre and with the variability of mode waters in the subtropical (Joyce et al. 2000) and subpolar (Chafik et al. 2016) basins.

The low-frequency component of the NAO reflects links with the North Atlantic decadal variability, which originates in the tropical and extratropical basins including the intergyre region and propagates across, and is often viewed as a response to atmospheric forcing and/or ocean dynamics (e.g., Deser and Blackmon 1993; Chang

et al. 1997; Tanimoto and Xie 1999; Ruiz-Barradas et al. 2000; Sutton et al. 2000; Marshall et al. 2001; Czaja et al. 2002; Guan and Nigam 2009; Deser et al. 2010; Buckley and Marshall 2016). Recent observational and modeling studies suggest that low-frequency variability of the NAO (Reintges et al. 2017; Álvarez-García et al. 2008) and, more generally, low-frequency variability in the North Atlantic (Delworth et al. 2017; Buckley and Marshall 2016) arise from the modulation of heat transports by the AMOC (Zhang 2017). The scope for interaction between the NAO, the GS's meridional excursions, and the AMO is considerable in view of the spatial proximity or even overlap of their key features in the North Atlantic basin, notwithstanding the separation of their canonical time scales. There is growing evidence that the AMO's SST anomalies can influence the NAO (Bjerknes 1964; Czaja and Frankignoul 2002; Rodwell and Folland 2002; Gulev et al. 2013; Peings and Magnusdottir 2016). Interestingly, the AMO-related winter height pattern resembles the NAO height anomalies (Kavvada et al. 2013), indicating an interaction pathway.

The fulcrum in the reported analysis is the index describing the latitudinal position of the northern wall of the GS at 200-m depth [as in Joyce et al. (2000)]. The analyzed datasets are briefly described in section 2. Lead-lag regressions on the GS index reveal the surface and subsurface evolution structure of the GS excursions (section 3), while lead-lag correlations of the GS index with the LF-NAO and the AMO tendency help characterize antecedence and subsequence vis-à-vis the AMO's decadal pulses (section 4). Support for the identified links from the similarity of suitably lead-lagged SST and SLP regressions on these indices and a discussion of feedbacks are also presented in section 4. Concluding remarks with a discussion of the fluctuation time scale (i.e., a mechanistic hypothesis for decadal fluctuations of the subpolar gyre) follow in section 5.

## 2. Datasets and methods

The Gulf Stream and the two regional modes of climate variability, the NAO and AMO, are referenced through their indices. The GS index, which tracks the position of the Gulf Stream's northern wall, was obtained from an empirical orthogonal function (EOF) analysis of the 15°C isotherm location at 200-m depth at selected locations within the 33°–43°N, 75°–50°W region. The 15°C isotherm, positioned approximately midway in the meridional temperature gradient ribbon to the north of the Gulf Stream's core, is a convenient marker for its northern "wall" (Fuglister 1963; Joyce et al. 2000). The GS index was provided by T. Joyce (2014, personal communication) as a smoothed, standardized, seasonal-resolution index for the

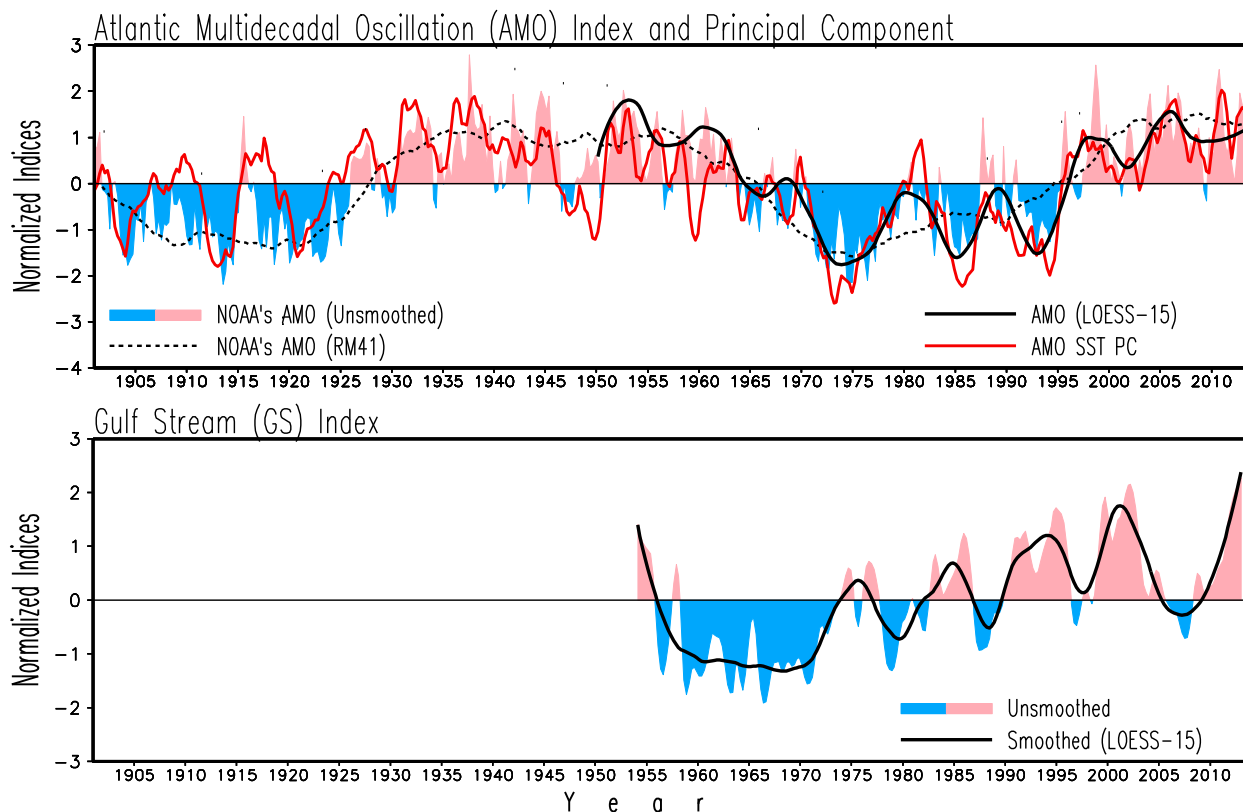


FIG. 1. (top) Atlantic multidecadal oscillation (AMO) and (bottom) Gulf Stream excursions (GS). NOAA's seasonally resolved AMO index (Enfield et al. 2001) is shown in red–blue and its 41-season running mean (RM41) by a dashed black line; the smoothed version is commonly used to highlight the AMO's multidecadal time scales. A less smoothed version, obtained from LOESS filtering (15% window over 1950–2013) and shown by the thick black line, brings out the decadal pulses present in AMO, e.g., the Great Salinity Anomaly of the 1970s. These pulses are evident in NOAA's unsmoothed AMO index (red–blue) and also prominent in the AMO SST principal component (thick red line), extracted from an extended-EOF analysis of spatiotemporal variability of seasonal SST anomalies (Guan and Nigam 2009). The Gulf Stream index (lower panel) tracks the meridional excursions of the Gulf Stream in the near-coastal longitudes (75°–50°W); it is based on the latitudinal location of the 15°C isotherm at 200-m depth (Joyce et al. 2000). The detrended and normalized seasonally resolved GS index is shown with red–blue shading while its LOESS-15 smoothed version is shown by a thick black line during 1954–2012, the period of index availability.

1954–2012 period. The index (Fig. 1) exhibits variability on interannual, decadal, and multidecadal time scales. The NAO index is based on the difference of normalized monthly sea level pressure between Lisbon, Portugal, and Stykkisholmur/Reykjavik, Iceland (Hurrell 1995); it depicts variability on subseasonal-to-decadal time scales, as noted earlier.

The AMO is generally defined as the linearly detrended, area-averaged SST anomaly in the northern Atlantic basin (0°–60°N, 75°–5°W), following Enfield et al. (2001). The NOAA AMO index (from NOAA's Earth System Research Laboratory), based on this definition, is shown in Fig. 1; both unsmoothed and smoothed versions are shown. Most literature references to the AMO are to its smoothed version (41-season running mean, RM41; dashed black line in Fig. 1, top panel), which highlights the multidecadal time scales—to the extent that this attribute is reflected in the

name of this variability mode (Kerr 2000). This heavy smoothing (RM41), however, suppresses, quite effectively, the robust decadal variability that is evident in the unsmoothed index (red–blue) and in the less heavily smoothed index versions (e.g., solid black line). The prominence of decadal pulses in AMO variability, of which the Great Salinity Anomaly of the 1970s is one example, was first noted by Guan and Nigam (2009), who identified them from objective analysis of seasonal SST anomalies, focusing on both temporal and spatial recurrence (e.g., extended-EOF analysis). The resulting SST principal component linked with AMO variability (Fig. 1, top panel, solid red line) captures both its decadal and multidecadal components. The decadal pulses so clearly manifest in NOAA's unsmoothed AMO index and in the AMO SST principal component are the focus of this analysis, which seeks to understand their genesis and development.

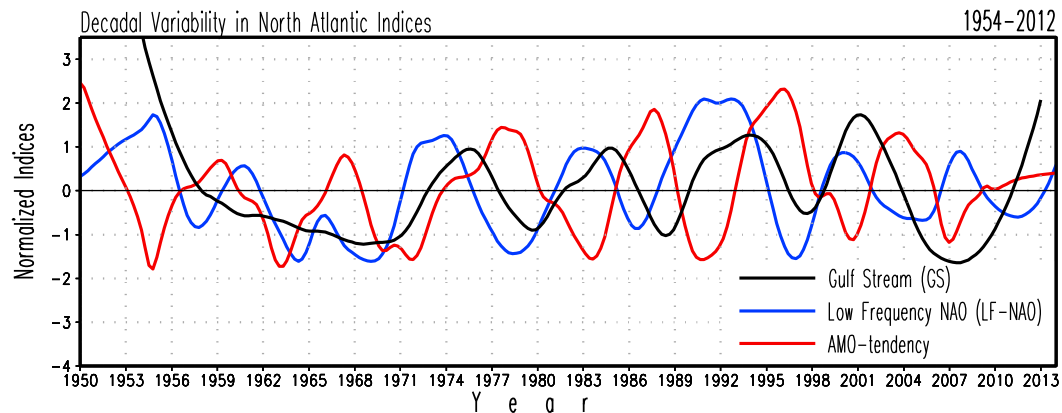


FIG. 2. Decadal variability of the subpolar gyre: The smoothed (LOESS-15) North Atlantic Oscillation index (blue; referred to as low-frequency NAO or LF-NAO) and Gulf Stream index (black) are plotted along with the AMO tendency [red;  $\partial(\text{AMO})_{\text{LOESS-15}}/\partial t$ ]. As discussed in text, the tendency measure implicitly highlights the shorter time scales, especially decadal pulses in the AMO context, but with introduction of a quadrature (quarter cycle) lead vis-à-vis the decadal pulses themselves. All three indices are detrended and normalized to facilitate visual lead-lag identification.

The atmospheric and oceanic fields analyzed in this study come from the UK Met Office's Hadley Centre for Climate Science. The sea level pressure data (HadSLP2; Allan and Ansell 2006) are available at monthly resolution on a  $5^\circ \times 5^\circ$  grid from 1850 to the present. Sea surface temperature data (HadISST, version 1.1; Rayner et al. 2003) are available at monthly resolution on a  $1^\circ \times 1^\circ$  grid from 1870 to the present. Subsurface ocean temperatures and salinity are from the EN.4.2.0 quality controlled objective analyses (Good et al. 2013) that were bias-corrected using the climatological *World Ocean Atlas 2009* (Levitus et al. 2009). Subsurface salinity and temperature, available on a  $1^\circ \times 1^\circ$  grid for the period of 1900 to the present, are used to calculate vertically averaged salinity for the 5–315-m layer and vertically integrated heat content for two layers: 5–315 m (upper ocean) and 315–968 m (deep ocean); sea surface salinity (SSS) refers to the salinity at 5-m depth.

A 20-yr mean dynamic topography from AVISO altimetry is used to characterize the mean position of the subpolar and subtropical gyres, and the Gulf Stream from the display of the  $-0.4$ ,  $0.4$ , and  $-0.1$ -m topography contours, respectively. This product is distributed by AVISO, with support from CNES (<http://www.avisio.altimetry.fr/duacs/>).

The reported analysis uses standard statistical tools such as lead-lag correlation and regression. Linear trend is evaluated using the least squares method. Seasonal data are analyzed and, unless otherwise noted, the indices are linearly detrended and standardized for the common 1954–2012 period, which is set by the availability of the GS index. The indices are smoothed, when noted, using the LOESS filter (Cleveland and Loader

1996) with a 15% span window (LOESS-15; i.e., with the window span being 15% of the 1954–2012 period, or  $\sim 9$  yr), which suppresses subseasonal-to-interannual variability while retaining the important decadal fluctuations. Statistical significance of the regressions and correlations is assessed by a two-tailed Student's  $t$  test at the 5% level using an effective sample size that accounts for serial correlation (Quenouille 1952); the significant regressed anomalies are stippled.

LOESS-15 filtering makes decadal variability more prominent in the AMO index but the intrinsic multi-decadal components of the index remain overwhelming (Fig. 1, top panel, solid black line). The AMO's decadal component (manifest in its decadal pulses) is thus “accessed” in this analysis through the index tendency,  $\partial(\text{AMO})/\partial t$ , which implicitly and conveniently highlights the higher frequencies, albeit with a temporal shift with respect to the AMO index, as shown in Fig. 2. The sensitivity of our findings to different span window choices in LOESS filtering is noted.

#### Smoothed indices

The linearly detrended, smoothed (LOESS-15), and normalized GS (black) and NAO (blue) indices are plotted in Fig. 2. LOESS-15 filtering has little impact on the GS index, which is dominated by decadal variability to begin with, but it is effective in the case of the NAO, yielding what will henceforth be referred to as the LF-NAO index. Also plotted is the tendency of the smoothed AMO index ( $\text{AMO}_{\text{LOESS-15}}$ , the black line in Fig. 1), specifically  $\partial(\text{AMO}_{\text{LOESS-15}})/\partial t$ , in red after normalization. The AMO tendency shows robust decadal variability, attesting to the efficacy of the tendency

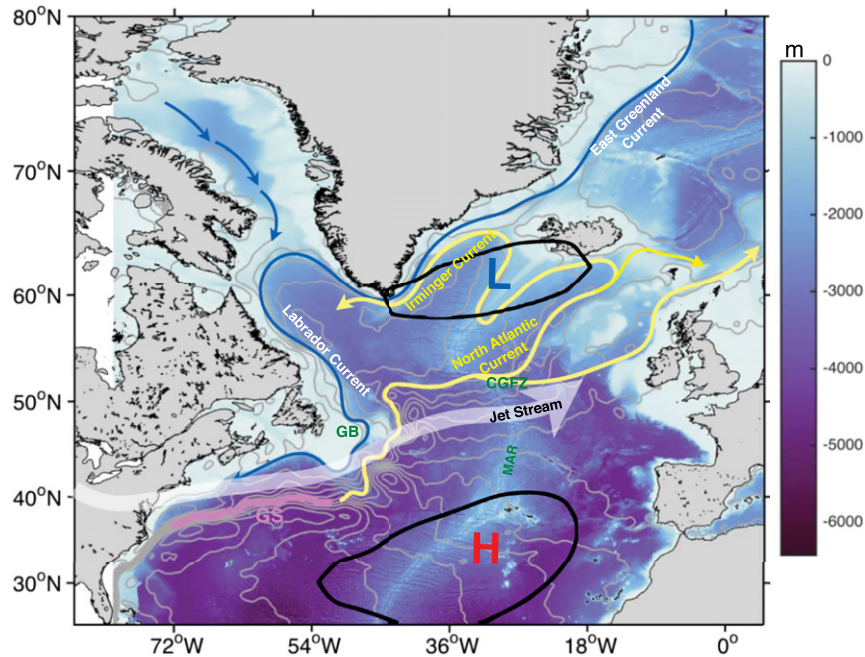


FIG. 3. Key bathymetric and ocean–atmosphere circulation features in the North Atlantic’s subpolar and subtropical basins. Ocean depth (m) is shown using a white (shallow) to blue (deep) color scale: The midbasin bathymetric rise running north–south, the Mid-Atlantic Ridge (MAR), and its interruption, the Charlie-Gibbs Fracture Zone (CGFZ), is marked; the extension of the North American continental shelf southeastward of Newfoundland, the Grand Banks (GB), is also marked. The displayed ocean circulation features include the time-mean absolute dynamic topography from 1993–2015 AVISO altimetry (gray contours every 0.1 m); the mean position of the Gulf Stream (GS; pink thick line) based on sea surface heights following the method by Pérez-Hernández and Joyce (2014); and the GS’s northward extension and the North Atlantic Current (yellow lines), which feed both the Nordic Seas (via the Norwegian Atlantic Current) and the Labrador Sea (via the Irminger Current) with warm and saline waters. Blue lines track the cold, fresh East Greenland and Labrador Currents that flow southward along continental boundaries/shelves. Depicted atmospheric circulation features include the Icelandic low (1006-hPa black contour around ‘L’), the Azores high (1020-hPa black contour around ‘H’), and the jet stream (mean axis of the 200-hPa isotachs, shown via a broad white transparent arrow), all from the 1954–2012 annual-mean NCEP–NCAR atmospheric reanalyses (Kalnay et al. 1996).

measure in extracting the decadal component from the multidecadal dominant AMO index. One, of course, needs to be cognizant of the quadrature delay between an oscillatory index and its tendency, with the tendency leading by a quarter-cycle; this phase difference will need to be factored in evaluations of temporal leads and lags with respect to the AMO’s decadal pulses.

### 3. The Gulf Stream System

The section begins with an overview of the bathymetric features in the subpolar basin and the regional atmospheric and oceanic circulations pertinent to the spatiotemporal development of Gulf Stream excursions (Fig. 3). Notable features include the Newfoundland basin to the southeast of the Grand Banks (GB), bounded on the east by the north–south-oriented Mid-Atlantic

Ridge (MAR); and the Charlie-Gibbs Fracture Zone (CGFZ), a MAR interruption generating east–west basin connectivity (with the northern ridge referred to as Reykjanes Ridge). Relevant atmospheric and oceanic circulation features are marked in Fig. 3 and discussed in its caption. The subpolar and subtropical gyres, identified from altimeter-based dynamic topography (plotted in Fig. 3), are marked on subsequent plots to provide tracking reference for GS evolution.

A comprehensive thermohaline view of the meridional displacements of the GS on decadal time scales is presented in Fig. 4, which shows the surface–subsurface regressions of temperature and salinity on the smoothed GS index over a 9-yr period spanning the pre- and postmature phase of GS excursions. The spatiotemporal development of the GS-related upper-ocean (5–315 m) heat content and salinity anomalies (middle columns) is

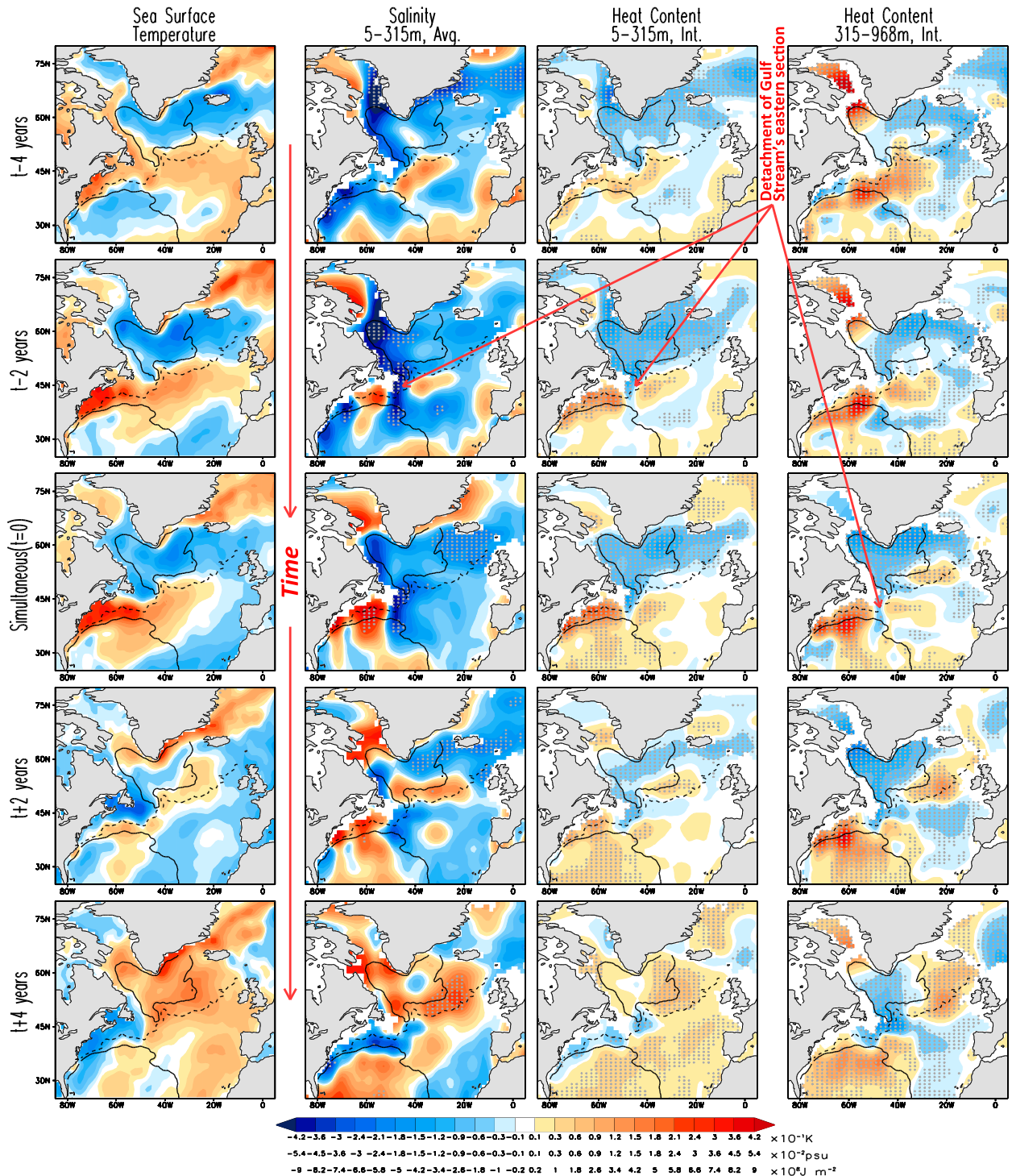


FIG. 4. Surface and subsurface evolution of Gulf Stream's meridional excursions. Lead-lag regressions of the temperature and salinity (from EN4.2.0 ocean analysis) on the smoothed (LOESS-15) GS index are shown to characterize the spatiotemporal development and decay of the GS's decadal excursions; regressions are for the 1954–2012 period, with simultaneous ones ( $t = 0$ ) in the middle row and the leading (lagging) ones above (below), i.e., with time running downward. Shown are (left) SST (K); (middle left), (middle right) upper-ocean salinity (5–315-m average; psu) and heat content (5–315 m integrated,  $\times 10^7 \text{ J m}^{-2}$ ), respectively; and (right) deep-ocean (315–968 m integrated) heat content. Orange and blue shading denotes positive and negative anomalies, respectively. Solid black lines mark the climatological annual-mean position of the subpolar and subtropical gyres using the  $-0.4\text{-m}$  and  $+0.4\text{-m}$  absolute dynamic topography values (from AVISO altimetry), respectively; the dashed black line tracks the climatological North Atlantic Current through the  $-0.1\text{-m}$  topographic contour. Initial detachment of the GS's eastern section from the southward intrusion of subpolar water is indicated by red arrows. Regions with statistically significant anomalies at the 5% level are stippled.

discussed prior to SST evolution because the GS index is based on subsurface temperatures. Note that in the near-coastal sector (westward of 50°W) the GS is strongest and most northward displaced in the upper-ocean heat content anomalies at  $t = 0$ , consistent with the location-sensitive GS index.

#### a. Mechanics of the subtropical–subpolar water exchange

The mature phase of the GS's northward displacement (Fig. 4, middle columns;  $t = 0$ ) is accompanied by a cold, fresh subpolar gyre (as in the AMO's cold pulses; e.g., the Great Salinity Anomaly of the 1970s; Slonosky et al. 1997), with gyre water leaking southward through the Newfoundland basin along the Grand Banks (~48°W), that is, well to the west of the Mid-Atlantic Ridge. The leakage of subpolar water is also evident in the  $t = 0$  deep-ocean (315–958 m) heat content regressions where it extends farther to the south. The leakage is perhaps stronger in the precursor phase ( $t - 2$  yr) when it is prominently manifest in upper-ocean salinity but only modestly in SST.<sup>1</sup> This southward leakage apparently cuts off an eastern section of the GS, first evident in the  $t - 2$  upper-ocean regressions and then in the  $t = 0$  deep-ocean heat content. Similar results (not shown) are obtained with the Ishii dataset (Ishii and Kimoto 2009).

The GS is not longitudinally stiff during meridional excursions. The nascent phase ( $t - 2$  yr) regressions of heat content exhibit a pinched-off/pinched section from the intrusion of cold subpolar water (from the gyre's western flank) into the Newfoundland basin along the Grand Banks; the preceding ( $t - 4$  yr) GS structure is, however, longitudinally coherent. The heat content regressions concurrent ( $t = 0$ ) with the northward displaced GS (middle row, last column) reveal a splitting off of the eastern section of the GS (marked by an arrow), and additional leakage of subpolar water through the Mid-Atlantic Ridge interruption between Iceland and the Azores (the Charlie-Gibbs Fracture Zone), which further splits the detached GS section into a northern and southern part (clearly manifest in the  $t = 0$  deep-ocean heat content; Fig. 4, middle row, right column). The postmature phase ( $t + 2$  and  $t + 4$  yr) consists of the northeastward displacement of the northern split section of the GS by means of the North Atlantic Current, which rises along its southwest-to-northeast trajectory (e.g., see Fig. 2 in Langehaug et al. 2012;

Burkholder and Lozier 2011).<sup>2</sup> The split section, located in the upper ocean after its transit, is in part entrained into the subpolar gyre from the eastern North Atlantic following the mean gyre circulation, leading to a warmer gyre at upper levels; the remaining anomaly continues into the Norwegian and Greenland Seas. The northeastward ascent of the North Atlantic Current apparently shields the deep levels of the subpolar gyre from intrusions of subtropical water as the northern split section of the GS rises during its cross-basin transit with the North Atlantic Current (the carrier current). The shielding of the subpolar gyre is indicated by the modest temporal variations of deep-ocean heat content in the gyre (Fig. 4, last column). The ascent of this carrier current can, perhaps, also account for the notable absence (presence) of the northern split section in the  $t = 0$  upper-ocean (deep-ocean) heat content, and its subsequent emergence in both upper- and deep-ocean heat content regressions.

A comparison of the  $t - 4$  and  $t + 4$  deep-ocean heat content regressions (Fig. 4, last column) shows striking evolution in GS structure, from an extended, coherent current with northeastward orientation at  $t - 4$  yr to a retracted, zonally oriented, southward displaced current with a broken-off eastern section at  $t + 4$  yr, or a decade later. The dynamic heights of the oceanic gyres provide pertinent reference in tracking the movement of the GS anomalies into the subpolar North Atlantic. The heat content regressions in Fig. 4 show that at  $t \leq 0$ , the warm anomaly in the upper-ocean heat content in the near-coastal sector is positioned to the north of the mean GS position (i.e., subtropical gyre boundary), but the warm anomaly that detaches from the GS is located south of the North Atlantic Current (NAC). After the GS's northern displacement in the western sector (i.e.,  $t > 0$ ), the detached anomaly is found to the north of the NAC along the mean absolute dynamic topography contour of the subpolar gyre. In the deep-ocean heat content regressions, however, the warm detached anomaly propagates along the NAC.

#### b. Statistical significance

Statistical significance of the regressions is assessed using the method outlined in section 2, with stippling denoting the significant anomalies in Fig. 4. It is immediately apparent that while the upper- and deep-ocean heat content anomalies are extensively significant (and to a lesser extent, the upper-ocean salinity anomalies), the SST anomalies are not assessed to be such. The lack of statistical significance in surface regressions (e.g.,

<sup>1</sup> The leakage is not manifest in SST, perhaps because of its direct exposure to the full spectrum of atmospheric variability via surface fluxes and related modulation, including “reddening” of the variability spectrum.

<sup>2</sup> The importance of the correct position of this current for generation of realistic Atlantic multidecadal variability in a climate model was recently noted (Drews and Greatbatch 2016).

SSTs) was neither unanticipated nor viewed as a setback for the analysis; in fact, it is its motivation. Such an outcome was anticipated because the ocean surface is exposed to myriad influences that can limit the significance of a weak but spatiotemporally coherent signal. The present analysis was designed to circumvent such difficulties by exploiting the spatiotemporal coherence residing in the subsurface fields. Not only are pertinent subsurface fields chosen for regression, they are also used in constructing the GS index, a key North Atlantic index with intrinsic decadal variability.

### *c. Influence of the low-frequency North Atlantic Oscillation*

It is noteworthy that the subpolar gyre is coldest and freshest in the upper layers (and surface) at  $t - 2$  yr (i.e., prior to the GS's northward displacement). This cold phase in the GS regressions, interestingly, is coincident with the LF-NAO's peak positive phase (cf. Fig. 2 and Figs. 5–8). This NAO phase, as noted earlier, consists of below normal sea level pressure (SLP) around Iceland and above normal SLP around the Azores (e.g., Nigam and Baxter 2015, their Fig. 4c; see also Fig. 8 herein), leading to a deeper Icelandic low in winter and thus strengthened westerlies over the subpolar gyre and stronger northwesterlies (northeasterlies) along Greenland's west (east) coast.<sup>3</sup> The NAO influences the surface wind speed, and thus sensible and latent heat fluxes, vertical mixing, and upper-ocean temperature over the subpolar gyre (Deser et al. 2010; Fig. 1). Along the coasts, the LF-NAO-related winds modulate coastal upwelling, impacting SST (Fig. 4, first column, second row). Cold SSTs along Greenland's west coast and warm SSTs off Baffin Island at  $t - 2$  yr (LF-NAO's peak positive phase) result from coastal upwelling and downwelling, respectively, induced by the LF-NAO northwesterlies, whereas the warm SSTs along Greenland's east coast arise from coastal downwelling generated by the LF-NAO northeasterlies. The coastally confined warm SSTs create the impression of a weakened East Greenland Current. SSTs can also change from ocean circulation and advection associated with the subpolar gyre, the Gulf Stream, and the North Atlantic Current, all of which have been shown to be important in generating decadal time scale variability in the North Atlantic (e.g., Visbeck et al. 2003; Zhang 2017) and for propagation of salinity anomalies (Dickson et al. 1988; Hátún et al. 2005).

<sup>3</sup> A positive phase of the NAO is associated with northeasterlies (and not southwesterlies) along Greenland's east coast because the closed low-SLP lobe of the NAO is centered over Iceland.

The coastal upwelling/downwelling origin of the SST anomalies around Greenland finds corroboration in related salinity, especially in the upper ocean where the upwelling regions are fresher and the downwelling ones saltier (e.g., at  $t - 2$  yr; Fig. 4), with the exception of the downwelling region east of Greenland where salty anomalies are not evident until  $t = 0$ , and even then only weakly, reflecting salinity suppression from the sea ice melt induced by warm SST anomalies in the Greenland Sea. The spatiotemporal evolution of the warm, salty anomalies in the Baffin Bay and Davis Strait is interesting as there is some indication of southward movement at the surface and subsurface, likely from advection by the Baffin Island and Labrador Currents, the latter of which strengthens during LF-NAO's positive phase (Han et al. 2014).<sup>4</sup> The southward descent of warm SST anomalies on both sides of Greenland, but especially along the east (from Greenland Sea) into the northern flank of the subpolar gyre, at  $t + 2$  yr sets the stage for LF-NAO's phase reversal, as argued later in the context of the hypothesis advanced for decadal fluctuations of the subpolar gyre. Note that there is little evidence for southward propagation of salinity anomalies along Greenland's east coast because of the compensation between the effects of downwelling and sea ice melt.

To sum up, lead-lag regressions on the GS index show decadal fluctuations in the GS's meridional location (in the western basin) to be associated with coherent upper-ocean heat content and salinity variations in the subpolar and subtropical gyre regions. The subpolar gyre is cold and fresh during GS's northward shift (as in the AMO's cold pulses) but not Baffin Bay and the Greenland and western Norwegian Seas. The GS's northward displacement is preceded (by 1–2 yr) by the LF-NAO's positive phase, as conclusively shown in the next section. The seed for LF-NAO's phase reversal, as argued more fully in subsequent sections, is sown by the LF-NAO itself through its induced SST anomalies and their interaction with regional currents.

## **4. The Gulf Stream's link with the LF-NAO and the AMO**

The Gulf Stream's link with LF-NAO variability and the AMO decadal pulses is analyzed in this section. The tripole structure of the GS-related SST anomalies (Fig. 4;  $t = 0$ ) is reminiscent of the NAO SST anomalies

<sup>4</sup> Concurrent with the southward movement of warm, salty anomalies in the Baffin Bay and Davis Strait is the exit of cold water from the Labrador basin into the Grand Banks, from where it moves southward along the American coast while defining the GS's northern boundary.

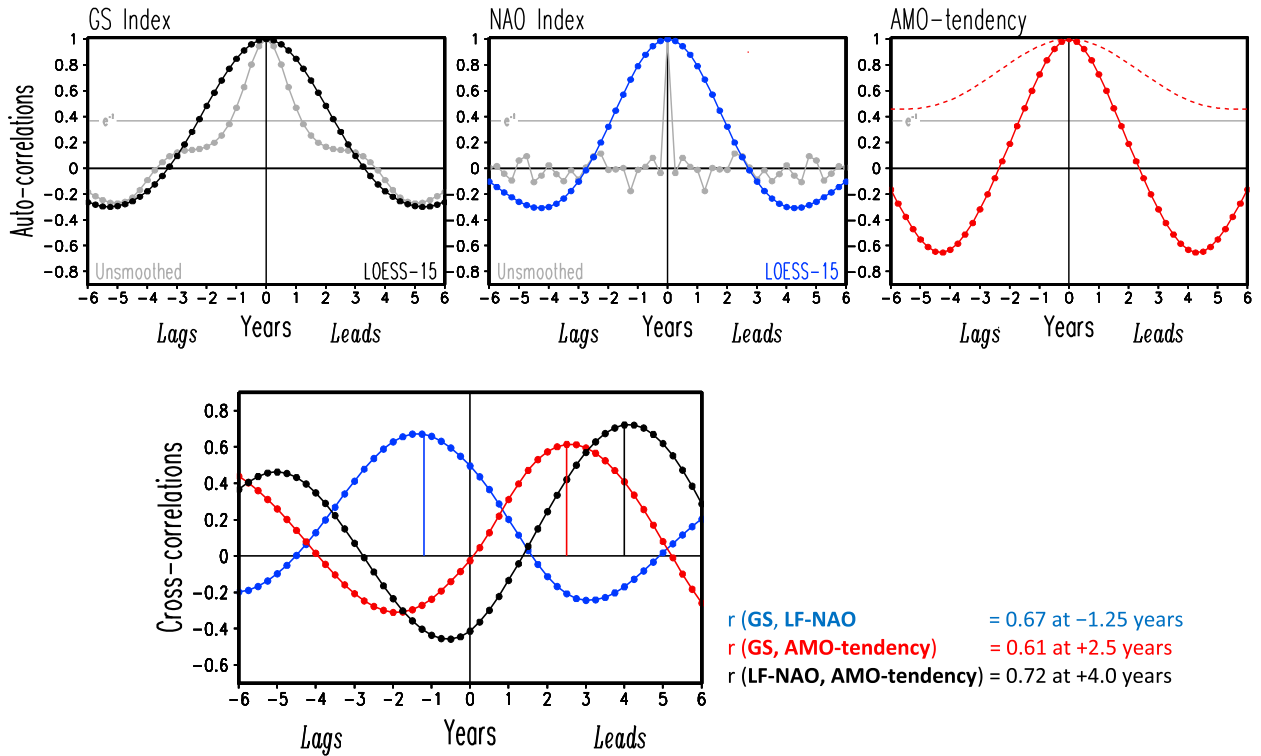


FIG. 5. Temporal relationship among indices. Autocorrelation of the smoothed and unsmoothed GS and NAO indices is shown in the top row. Autocorrelation of the AMO tendency (Fig. 2, red curve) is shown in the top-right panel (red dots), which also shows the autocorrelation of the  $(\text{AMO})_{\text{LOESS-15}}$  index (dashed red) to draw attention to the shorter time scales of the tendency index. Cross-correlations of the indices are displayed in the bottom panel, with the convention that if  $r(A_t, B_{t+\tau}) > 0$  for  $\tau > 0$  ( $\tau < 0$ ), then  $A$  leads (lags)  $B$ . Also,  $r(\text{GS}, \text{LF-NAO})$  is shown in blue,  $r(\text{GS}, \text{AMO tendency})$  in red, and  $r(\text{LF-NAO}, \text{AMO tendency})$  in black. The lead-lag  $\tau$ -value at which  $|r|$  is largest is marked by a vertical line and the related  $\tau$  and cross-correlation values noted: low-frequency NAO variability leads the Gulf Stream's northern excursions by  $\sim 1.25$  yr and the AMO tendency by  $\sim 4$  yr, consistent with the  $\sim 2.5$ -yr lead found for Gulf Stream's northern excursions over AMO tendency. The horizontal gray line labeled  $e^{-1}$  in the top panels indicates an autocorrelation value of  $0.37 (=1/e)$ , which is a commonly used decorrelation threshold.

(e.g., Marshall et al. 2001, Fig. 2a therein; Nigam 2003, Fig. 6 therein; Deser et al. 2010, Fig. 1a therein) and to an extent also of the AMO's negative phase SST anomalies, especially in the eastern half of the basin (e.g., Guan and Nigam 2009, Fig. 4c therein). A link between the GS and LF-NAO, with the GS lagging by 0–2 yr, has been noted before (Joyce et al. 2000; Hameed and Piontkovski 2004; Sanchez-Franks et al. 2016) but not the GS or LF-NAO's association with the AMO's decadal pulses.

That the GS, LF-NAO, and AMO tendency indices are related is visually apparent from their temporal distribution (Fig. 2): The LF-NAO is seen leading the GS index by 1–2 yr in the swarm of decadal pulses beginning in the 1970s, whereas the AMO tendency is found lagging the LF-NAO by  $\sim 4$  yr across the record.

The dominant time scales implicit in the unsmoothed and smoothed indices are revealed from the autocorrelation structure of the GS and NAO indices (Fig. 5, top row). LOESS-15 smoothing evidently has limited impact on the GS index whose autocorrelation structure indicates a

dominant time scale of 9–13 yr; the range is estimated from twice the temporal distance between the  $e^{-1}$  and zero crossings of the autocorrelation. Autocorrelation of the NAO index, on the other hand, is very sensitive to smoothing, as anticipated. For characterization of the subpolar–subtropical water exchange, the smoothed NAO index (LF-NAO) with dominant time scales of 8–11 yr is the one of interest. The autocorrelation structure of the AMO tendency reveals its dominant time scales to be 7–9 yr, consistent with estimations of pulse duration in the raw and smoothed AMO indices (Fig. 1, top panel).

#### a. Links between indices

A quantitative underpinning to the links between the indices is provided in the bottom panel of Fig. 5 from computation of the cross-correlation at various leads and lags: Considering the entire record, and not just the four decadal pulses, the LF-NAO is found to lead GS variability by  $\sim 1.25$  yr (5 seasons) and the AMO tendency by 4 yr; not surprisingly, GS leads the AMO

tendency by  $\sim 2.5$  yr. The cross-correlations at these leads/lags, noted in the legend of Fig. 5, are all greater than 0.6 and statistically significant; the critical values at the 95% level of significance between the smoothed, detrended indices at these leads/lags are  $r(\text{GS}, \text{LF-NAO}) = 0.49$ ,  $r(\text{GS}, \text{AMO tendency}) = 0.53$ , and  $r(\text{LF-NAO}, \text{AMO tendency}) = 0.63$ . The critical value ( $r_c$ ) is obtained using the large-sample normal approximation:  $r_c = 2/[\sqrt{df - |\text{mlag}|}]$ , with  $df$  being the degrees of freedom, and  $\text{mlag}$  is the lead/lag at which the correlation is maximum.

Assuming the AMO decadal pulses to be of 8-yr duration (the central value of the above estimated 7–9-yr time scale), a quadrature cycle would be 2 yr. This would result in the LF-NAO and GS leading the AMO's decadal pulses by 6.0 and 4.5 yr, respectively. The lead–lag relationships are relatively insensitive to the choice of window span in LOESS filtering; for example, with LOESS 10% (20%) smoothing, LF-NAO's lead over the GS is 1.0 (1.5) yr. The lead–lag links suggest that LF-NAO's peak positive phase—with low SLP over Iceland and a cold, fresh subpolar gyre—precedes the GS's northward displacement by  $\sim 1.25$  yr, and that  $\sim 4.5$  yr after this displacement the subpolar gyre, Greenland Sea, and the eastern basin exhibit warm SST anomalies resembling aspects of the AMO's middle-to-high-latitude SST pattern. This cold-to-warm phase transition of the subpolar gyre is, of course, affected by the subtropical–subpolar water exchange processes characterized in section 3.

The temporal leads and lags are schematically summarized in Fig. 6 where the LF-NAO, the GS's meridional excursions, and the AMO's decadal pulses are represented as cyclical processes using circles (inner blue, middle black, and outer red), with radial lines marking the peak positive phase and the solid-to-dashed change in circumference lines representing phase transitions. LF-NAO's temporal lead over the other two processes (i.e., its orchestrator role) led to it being drawn as the inner circle—the driver of decadal fluctuations of the subpolar gyre.<sup>5</sup> Such a leading role would, of course, warrant elucidation of the mechanisms that generate phase transition in LF-NAO (indicated by points A and C in Fig. 6); the elaborate figure caption has more details. A potential mechanism for the phase transition is discussed in section 5 (using Fig. 9).

The next subsection seeks corroboration of the above-noted temporal phase relationships between the three indices in the lead-lagged fields of key ocean–atmosphere interface variables: SST (oceanic) and SLP (atmospheric).

### b. Spatiotemporal development of surface anomalies

Structural similarities in the ocean–atmosphere surface anomalies related to the LF-NAO, GS, and the AMO tendency at various leads and lags are highlighted in support of the temporal lead–lag relationships noted above. SST regressions on the three indices, each over a 7-yr period, are shown first (Fig. 7) with time running downward but with columns shifted vertically to reflect the lead–lag between indices; such shifting should facilitate recognition of similar spatial structure across the columns. The center column shows the GS-related SST development in view of the GS's key role in linking antecedent LF-NAO variability (left column) with the subsequent AMO tendency (right column); the GS-related SST development was also shown earlier (Fig. 4, left column).

The cross-column correspondence in SST regressions (Fig. 7) is notable, reflecting the significant lead–lag correlation ( $>0.6$ ) among the indices (Fig. 5, bottom panel): For example, in the row displaying simultaneous SST regressions on the GS index (third from the top), a warm Baffin Bay, cold subpolar gyre, warm Greenland Sea, northward displaced Gulf Stream, and cooler eastern and tropical Atlantic are found in all three panels. The correspondence, however, is not always as extensive; for example, in the following row, the subtropical Atlantic is warm across the basin in only the last column, despite cross-column similarities elsewhere. Some lack of correspondence undoubtedly emerges from the use of a 3-yr lag (and not 2.5 yr, as estimated in Fig. 5, bottom panel) for the AMO tendency vis-à-vis the GS index.

The lead–lag relationships between the important modes of decadal variability in the North Atlantic—the LF-NAO, GS displacements, and the AMO decadal pulses—is buttressed from SLP regressions in Fig. 8; select contours of the climatological winter SLP field are superposed in all panels for positional reference. The LF-NAO's SLP regressions are strong in both  $t - 1$  and  $t + 1$  yr (not surprisingly, as these periods are closest to the mature phase,  $t = 0$ , which is not shown), with the low off the southern tip of Greenland positioned close to the wintertime Icelandic low; the LF-NAO's low is only  $\sim 1$  hPa deep.<sup>6</sup> The high SLP feature is centered northward of the Azores high, modestly shifting the climatological surface westerlies northward. The 7-yr evolution displayed in Fig. 8 does not fully cover a LF-NAO episode (of 8–11-yr duration) but it does show, interestingly, that phase reversal is initiated in the Norwegian and Greenland Seas where the low-to-high

<sup>5</sup> Tagging any one process as the driver in a coupled oscillatory system would be arbitrary, but the LF-NAO is tagged here to facilitate discussion of the process sequence.

<sup>6</sup> SLP regressions on the monthly NAO index are  $\sim 7$  hPa in the same region (e.g., Nigam 2003).

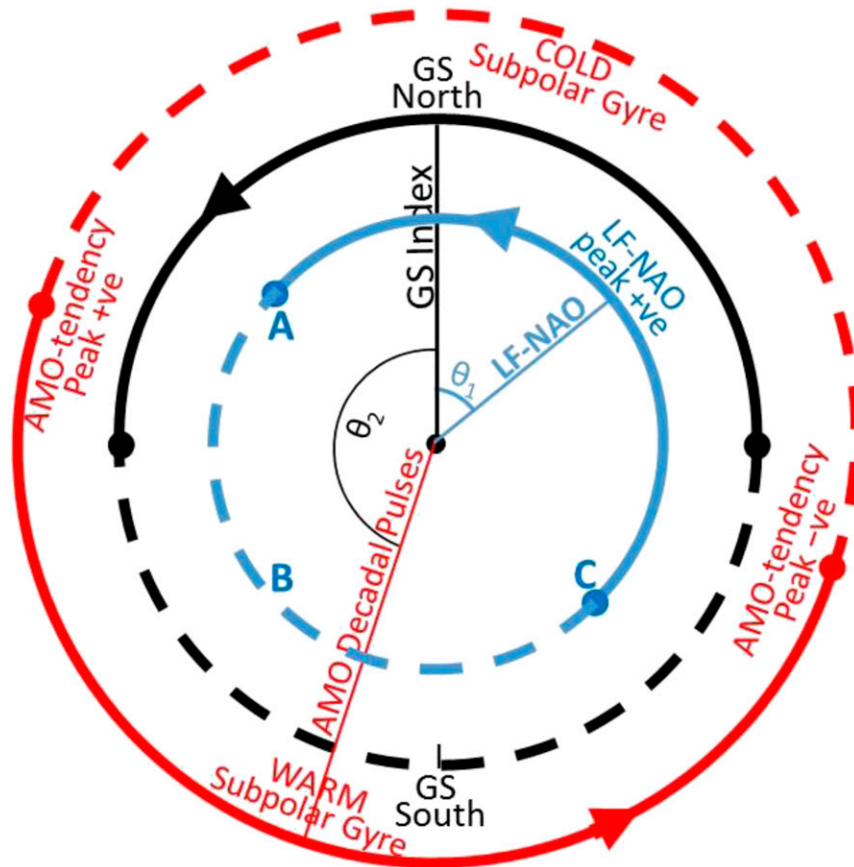


FIG. 6. Schematic depiction of the temporal phasing of the key processes generating decadal variability of the subpolar gyre, based on observational analyses reported in the preceding figures: the low-frequency North Atlantic Oscillation (LF-NAO; blue circle), the Gulf Stream's meridional excursions (GS; black circle), and the AMO's decadal pulses (red circle). Time runs counterclockwise, with solid (dashed) arcs denoting the positive, +ve (negative, -ve) oscillatory phase, and solid dots marking phase transitions. Radial lines point to the peak +ve phase of each oscillation, and the angle between these lines indicates the temporal lead/lag between them. The LF-NAO's peak +ve phase (marked by a deeper Icelandic low) occurs prior ( $\sim 1.25$  yr) to the northward displacement of the Gulf Stream, i.e., LF-NAO leads GS by  $\theta_1 [\approx 2\pi(1.25/T)]$  radians. The GS leads the AMO's decadal pulses by  $\sim 4.5$  yr, i.e.,  $\theta_2 [\approx 2\pi(4.5/T)]$ ; note that GS leads AMO tendency by  $\sim 2.5$  yr (cf. Fig. 5), which, in turn, has a quadrature lead ( $\sim 2$  yr) over the AMO's decadal pulses, leading to the 4.5-yr lead. The oscillatory period of the subpolar gyre ( $T$ ) in this schematic is 10 yr, a central value in the estimated fluctuations time scales (7–13 yr; see text). It is noteworthy that the Gulf Stream's northward displacement is nearly concurrent with the peak cold phase of the subpolar gyre. As the LF-NAO (atmospheric variability) leads both GS and the AMO tendency (subsurface and surface oceanic variabilities), process-level insights on how its own phase reversal is generated from regional ocean–atmosphere interactions at points A and C will help advance understanding and modeling of subpolar gyre variability (see Fig. 9 and related text).

SLP change in subpolar latitudes is first manifest (e.g., at  $t + 3$  yr; fourth row). The phase reversal is not fully resolved in the displayed LF-NAO regressions but it is in the GS ones, where it supports the assertion of the phase reversal initiation in the Norwegian Sea.

It is noteworthy that SLP anomalies over the subpolar gyre are not thermodynamically inferable from the underlying SST anomalies (from their influence on boundary layer temperature and hydrostatic balance), as evident

from the overlap of cold SST and low SLP anomalies in the gyre region in the  $(t + 1)$  LF-NAO regressions (Figs. 7 and 8). The influence, in fact, is often in the other direction, with the SLP anomalies and related surface winds and the wind-impacted surface fluxes influencing SST (e.g., Deser et al. 2010), leaving unanswered the question on how SLP variations over the subpolar gyre are generated. SLP here can, of course, readily vary from the displacement of the Atlantic storm tracks (and related feedback; i.e., from

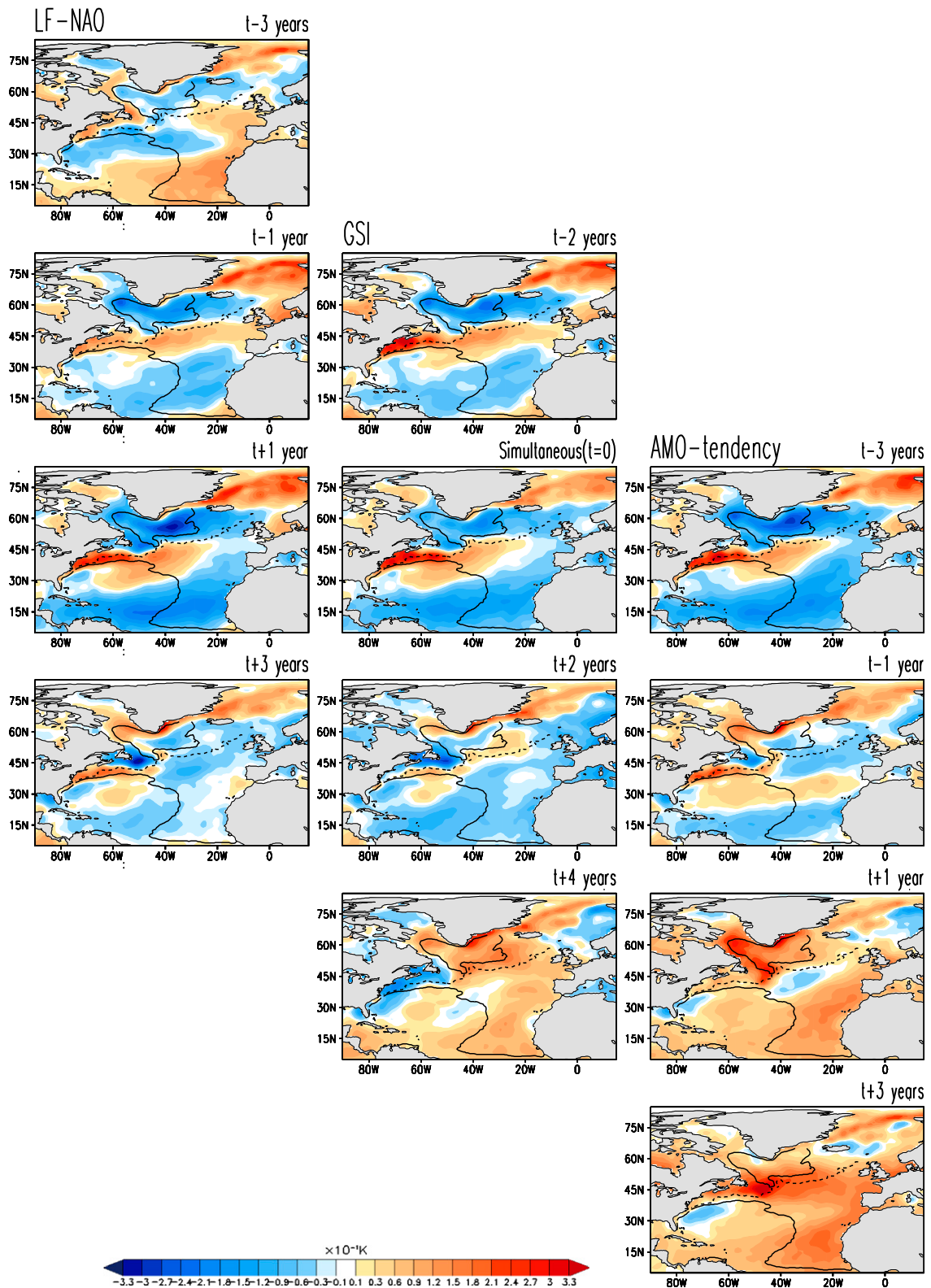


FIG. 7. Lead-lag regressions of SST on the (left) LF-NAO, (middle) GS, and (right) AMO tendency indices. Regressions are displayed at 2-yr intervals with time running downward, and with the columns shifted vertically to reflect the lead/lag between indices (identified in Fig. 5); regressions are for the 1954–2012 period. Negative SST anomalies are shaded blue and the positive ones orange. Black lines mark the climatological position of the subpolar and subtropical gyres and the North Atlantic current.

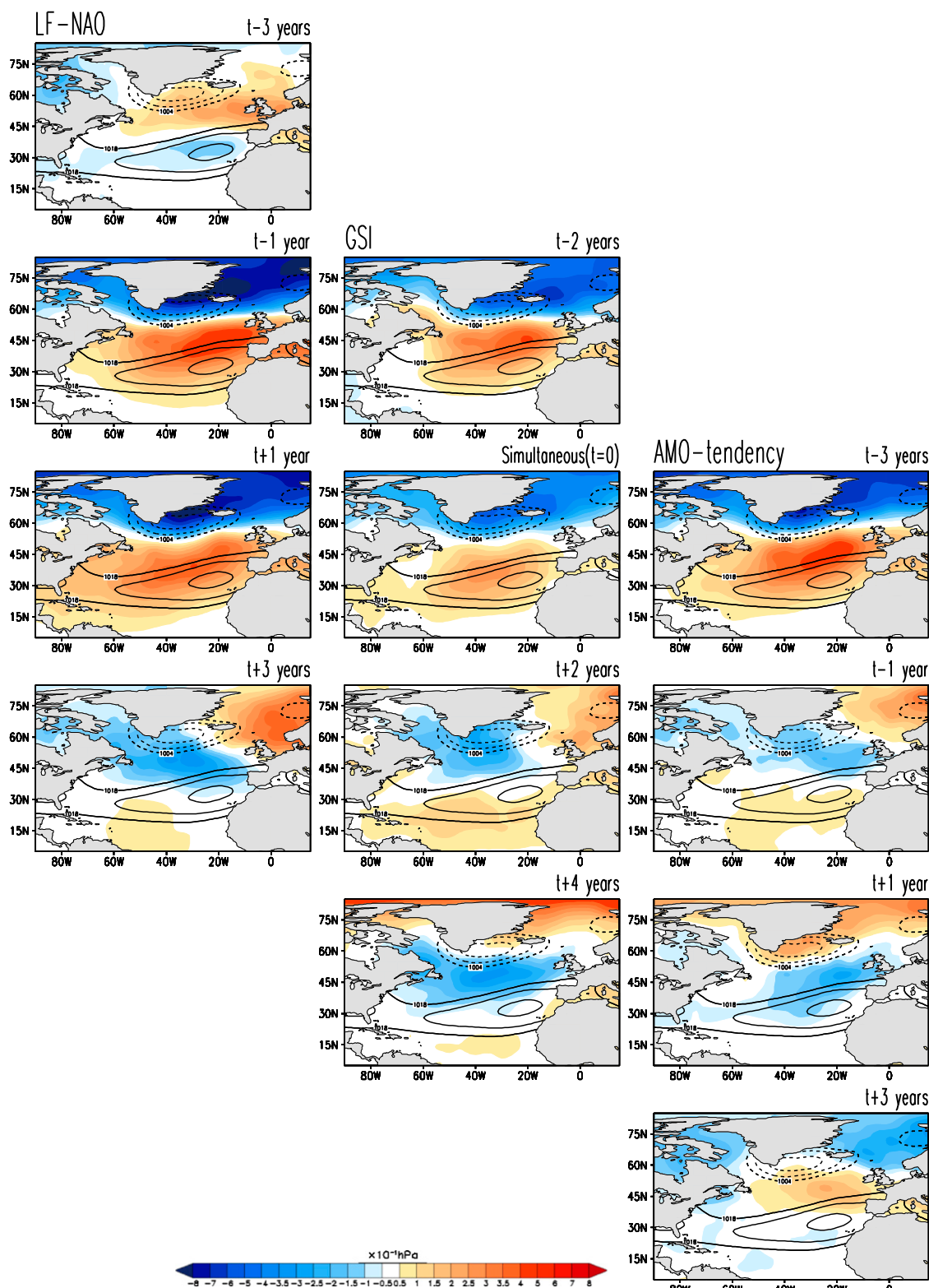


FIG. 8. Lead-lag regressions of sea level pressure (SLP) on the (left) LF-NAO, (middle) GS, and (right) AMO tendency indices. Regressions are displayed at 2-yr intervals with time running downward, and with columns shifted vertically to reflect the lead/lag between indices (identified in Fig. 5); regressions are for the 1954–2012 period, in hPa. Negative SLP anomalies are shaded blue and the positive ones orange; see scale. Black lines mark the climatological winter position of the Icelandic low and the Azores/Bermuda high, with contour labels in hPa.

dynamical mechanisms), as discussed later in this section (see also Nigam and Chan 2009).

The row containing simultaneous SLP regressions on the GS index (Fig. 8, third from the top) exhibits striking cross-column correspondence over the subpolar and subtropical gyre and the Norwegian Sea, as with SST regressions (Fig. 7). There is considerable cross-column similarity in the other rows as well, supporting the identified phase relationships among LF-NAO, GS displacements, and the AMO decadal pulses.

### c. The LF-NAO feedback

The temporal lead–lag relationships (or phase differences) among key processes generating decadal fluctuations of the subpolar gyre (i.e., the AMO’s decadal pulses) are summarized in Fig. 6. The schematic is however silent on the feedback of the LF-NAO-influenced ocean state on the overlying atmosphere, particularly on LF-NAO’s evolution, including its phase change (e.g., point A in Fig. 6). Knowledge of this feedback would be essential for advancing understanding of the mechanisms generating gyre oscillations, especially in view of LF-NAO’s temporal phase lead over other processes. The feedback on LF-NAO evolution is documented in Fig. 9, which shows the latitude–height structure of the tropospheric zonal wind and temperature regressions on the LF-NAO index, averaged over the Atlantic sector ( $60^{\circ}\text{W}$ – $0^{\circ}$ ). Consistent with LF-NAO’s impact on SST (Fig. 7, left column; e.g., at  $t + 3$  yr), which consists of warm anomalies on either side of Greenland and along the northern flank of the subpolar gyre,<sup>7</sup>  $\partial T/\partial y$  is positive over the subpolar gyre, weakening the overlying westerlies from thermal wind balance. The temperature and wind regressions in Fig. 9 (e.g., at  $t + 3$  yr) indeed capture the development of positive  $\partial T/\partial y$  and easterly wind anomalies over the gyre, with the development extending well into the upper troposphere. The resulting southward shift of the tropospheric jet (and storm tracks) is only a reflection of the LF-NAO phase transition (e.g., Peings and Magnusdottir 2016); feedback from storm track diabatic heating and transients on regional SLP (Hoskins and Valdes 1990) will contribute further to the buildup of the negative phase of the LF-NAO.

The mechanisms by which warm SSTs in the seas around Greenland warm the overlying atmosphere were

<sup>7</sup> The warm SSTs consists of the ones in Baffin Bay that descend into the Labrador Sea and get entrained into the northwestern flank of the subpolar gyre. To the east, warm SSTs are present in the Greenland and Norwegian Seas with extensions into the Denmark Strait and Irminger Sea, and subsequent entrainment into the northern flank of the subpolar gyre.

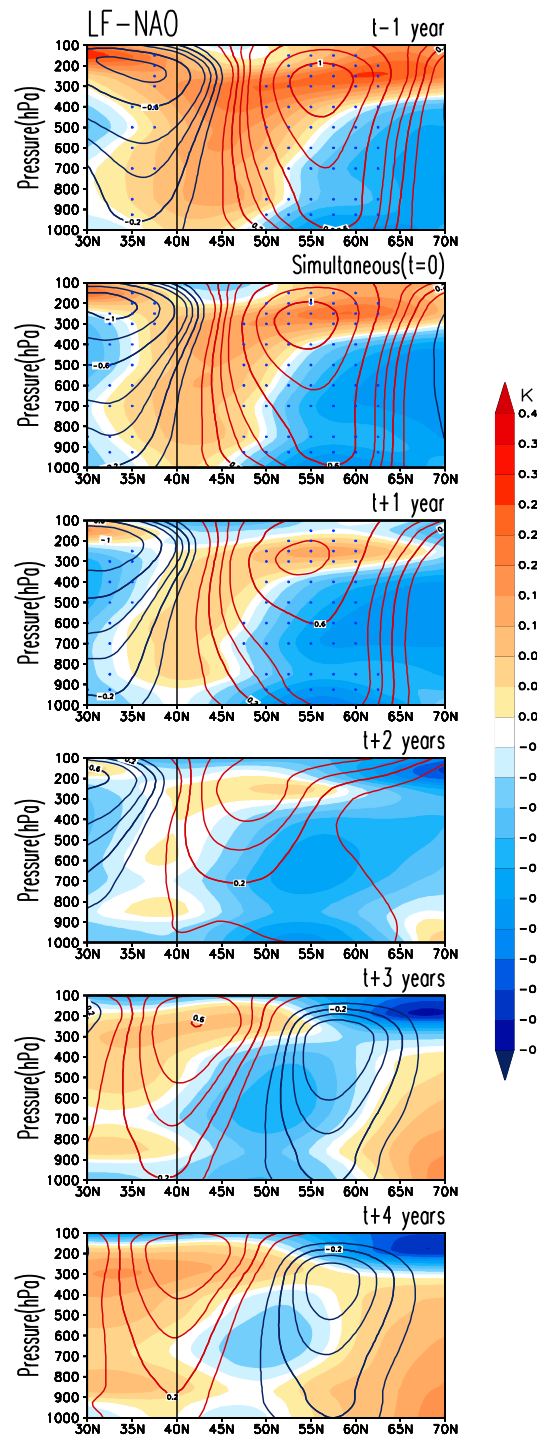


FIG. 9. Latitude–height structure of the temperature and zonal wind regressions on the LF-NAO index (shown in Fig. 2, top panel, blue line); the regressions are averaged across Atlantic longitudes  $60^{\circ}\text{W}$ – $0^{\circ}$ , and based on 1954–2012 NCEP reanalysis data. Temperature is shaded (negative values in blue) at  $0.04\text{-K}$  interval beginning at  $\pm 0.01\text{ K}$ ; see the side color bar. Zonal wind regressions are contoured in black (negative) and red (positive) with an interval of  $0.1\text{ m s}^{-1}$  in the  $0.1$ – $0.4\text{ m s}^{-1}$  range and  $0.2\text{ m s}^{-1}$  thereafter. Statistically significant zonal wind regressions at the 5% level are stippled. The climatological position of the subtropical jet in the western Atlantic ( $\sim 40^{\circ}\text{N}$ ) is marked by the black vertical line.

briefly examined, principally through computation of the lead–lag regressions of the surface heat flux on the LF-NAO index. Although not shown, the flux regressions at  $t + 3$  (and later) years were upward, supporting the warming of the regional lower troposphere at the expense of the underlying ocean surface temperatures, consistent with the surface-focused vertical structure of temperature regressions in Fig. 9 (bottom panels). This is also broadly consistent with the findings of observational studies on how the influence of the midlatitude and subpolar Atlantic SST anomalies is conveyed aloft [e.g., Czaja and Frankignoul 2002; Czaja and Blunt 2011; see especially Gastineau and Frankignoul (2015), who show how the AMO-related SST anomalies modify the strength of the atmospheric circulation through shifts of the baroclinic zone].

### 5. Mechanistic hypothesis and concluding remarks

Decadal pulses are an integral and influential feature of the Atlantic multidecadal oscillation (AMO), whose common references focus on its multidecadal component, a 60–70-yr oscillation in the North Atlantic basin-averaged SST. The decadal pulses are seldom recognized or studied because the basin-averaged SST anomaly (the AMO index) is customarily displayed after heavy smoothing that filters the pulses; an example is NOAA’s widely referenced AMO Index (RM41; Fig. 1, dashed black line). The pulses are however evident in both raw (i.e., unsmoothed) and less smoothed index versions (Fig. 1, red–blue shading and black line, respectively) and also prominent in the AMO-related SST principal component (Fig. 1, solid red line; no smoothing applied) that was objectively extracted on the basis of spatial *and* temporal recurrence of seasonal SST anomalies (Guan and Nigam 2009). A series of decadal pulses (2 to 3, typically) populate each multidecadal phase of the AMO, indicating robustness of the constituent decadal variability.

The origin of the AMO’s decadal pulses, which represent decadal variability of the subpolar gyre, is sought in the spatiotemporal evolution of the modes of variability having footprints in the extratropical basin—one atmospheric (NAO; especially, its low-frequency component, LF-NAO) and one oceanic (the Gulf Stream’s meridional excursions, captured by the subsurface temperature–based GS index). The AMO’s decadal pulses were “accessed” in this analysis not by filtering the AMO index but through its tendency,  $\partial(\text{AMO})/\partial t$ . The tendency measure was effective in extracting the shorter time scales but, as expected, temporally shifted (quarter-cycle lead) with respect to the decadal pulses themselves.

Lead–lag regressions of the *observed* surface/subsurface temperature and salinity (EN4.2.0 ocean analysis) on the LF-NAO and GS index reveal the mechanics of the subtropical–subpolar water exchange. The exchange is initiated and orchestrated by the LF-NAO whose geographic reach is extensive—from subpolar to subtropical latitudes, and across continents and oceans in longitude—leading to coordinated (but, often, unrelated) changes in the seas around Greenland (Baffin Bay, Davis Strait, Labrador Sea, Irminger Sea, and the Greenland and Norwegian Seas) and, of course, in the subpolar and subtropical gyres. The northern changes can be broadly characterized as being more surface-driven (sensible and latent heat flux, coastal upwelling, Ekman transports, and sea ice melt; e.g., Deser et al. 2010) whereas the southern ones are more influenced by ocean bathymetry (e.g., leakage of subpolar water through the Newfoundland basin and the Charlie-Gibbs Fracture Zone, and subsequent detachment of the Gulf Stream’s eastern section) and ocean circulation, especially the meridional excursions of the GS and the cross-basin transit of the GS’s detached eastern section via the North Atlantic Current.

The temporal lead–lag relationships (or phase differences) among key processes generating decadal fluctuations of the subpolar gyre (i.e., the AMO’s decadal pulses) are summarized in Fig. 6. The feedback of the LF-NAO-influenced oceanic state on the atmosphere overlying the northern basin is documented through tropospheric temperature and zonal wind regressions in Fig. 9. The feedback, affected by the heating of the lower troposphere by the underlying SSTs (as confirmed by examination of the sign of related surface heat flux regressions) and the thermal wind–related zonal jet displacement, is important for the phase transition of the LF-NAO (i.e., for its transit through point A in Fig. 6). Estimating the feedback time scale along with the cross-basin transit time of the GS’s detached eastern section should advance understanding of the subpolar gyre oscillations mechanisms, especially in view of the LF-NAO’s temporal lead over other processes.

#### a. Mechanistic hypothesis

An emergent view from this observational analysis of the upper-ocean thermal and salinity fields, especially from the temporally phased structures linked with key variabilities in the North Atlantic—the low-frequency NAO and the Gulf Stream’s meridional excursions in the western basin—is that decadal fluctuations of the subpolar gyre (representing the AMO’s decadal pulses) can be generated from a phased process sequence as shown below.

- Begin with the positive phase of the LF-NAO, with below (above) normal SLP to the north (south). While

the northern lobe is collocated with the Icelandic low, the southern one is positioned northward of the Azores high (cf. Fig. 8). Ekman transports induced by the LF-NAO winds will perturb both gyres, moving the gyre boundary (or Gulf Stream) northward.

- A perturbed (stronger) subpolar gyre concurrently leads to the detachment of the GS's eastern section from the southward intrusion of subpolar water through the Newfoundland basin (Fig. 4; red arrows); the detached section moves northeastward along the southeastern flank of the subpolar gyre.
- The gyre fluctuation time scale is determined, in part, by the time taken by the GS's detached eastern section to transit from the western basin ( $\sim 40^\circ\text{N}$ ,  $\sim 50^\circ\text{W}$ ) to the eastern flank of the subpolar gyre ( $\sim 50^\circ\text{N}$ ,  $\sim 30^\circ\text{W}$ ). The transit time is  $\sim 5$  yr [see Fig. 4, third column; from  $(t - 2)/(t = 0)$  to  $(t + 4)$  yr], leading to a gyre oscillation period of  $\sim 10$  yr, in accord with the dominant time scale of the AMO tendency (7–9 yr) and GS excursions (9–13 yr).
- The seed for LF-NAO phase reversal is sown, in large part, by the LF-NAO itself, through its impact on the SSTs around Greenland and their influence on tropospheric temperatures and thermal wind. This self-feedback of the LF-NAO, consequential given its temporal lead over other pertinent processes, also contributes in setting the gyre oscillation time scale.

#### b. Detachment of the Gulf Stream's eastern section

An interesting finding reported in this paper is the detachment of the Gulf Stream's eastern section on decadal time scales. The detachment apparently results from the intrusion (or leakage) of subpolar (cold, fresh) water into the Newfoundland basin along the Grand Banks, continuing into the Gulf Stream region and the subtropics. The intrusion is crucial for the pinching off of salinity and heat content anomalies (i.e., detachment) that continue into the northeast Atlantic region. The detachment of the Gulf Stream's eastern section has not been noted before, at least, in the context of basin-scale ocean circulation and its decadal variability. Interestingly, Bower et al. (2013) show eddies with subpolar characteristics to penetrate deeply into the subtropics in exactly the same region where the intrusion of subpolar waters occurs in this analysis.<sup>8</sup> The intrusion is located where the continental slope is steep, which induces instabilities of the boundary current, promoting generation of eddies.

<sup>8</sup> Bower et al. analyzed floats at 700–1500-m depths, with only 3 of the 59 deployed floats crossing the Gulf Stream.

Our analysis indicates that decadal fluctuations of the subpolar gyre (i.e., the AMO decadal pulses) involving notable salinity and heat anomalies result from a complex process sequence involving surface flux forcing, coastal upwelling, Ekman transports, ocean circulation, and the no less important bathymetric influences—and not merely from stochastic atmospheric forcing of a slab ocean (Clement et al. 2015).

Can the AMO's multidecadal time scales be generated from the rectification of the decadal variability fluxes? This intriguing question, along the lines of synoptic eddy feedback on supersynoptic and subseasonal atmospheric variability, will be the focus of a subsequent investigation.

*Acknowledgments.* The authors thank Terry Joyce for providing the updated Gulf Stream index. Sumant Nigam and Alfredo Ruiz-Barradas gratefully acknowledge the support of the U.S. National Science Foundation through Grant AGS1439940. Léon Chafik acknowledges funding through the iNCREASE project. Argyro Kavvada performed preliminary analysis of the GS and NAO links as part of her doctoral thesis to the University of Maryland, submitted and defended in May 2014.

#### REFERENCES

- Allan, R., and T. Ansell, 2006: A new globally complete monthly historical gridded mean sea level pressure dataset (HadSLP2): 1850–2004. *J. Climate*, **19**, 5816–5842, <https://doi.org/10.1175/JCLI3937.1>.
- Álvarez-García, F., M. Latif, and A. Biastoch, 2008: On multidecadal and quasi-decadal North Atlantic variability. *J. Climate*, **21**, 3433–3452, <https://doi.org/10.1175/2007JCLI1800.1>.
- Bjerknes, J., 1964: Atlantic air–sea interaction. *Advances in Geophysics*, Vol. 10, Academic Press, 1–82, [https://doi.org/10.1016/S0065-2687\(08\)60005-9](https://doi.org/10.1016/S0065-2687(08)60005-9).
- Booth, B. B. B., N. J. Dunstone, P. R. Halloran, T. Andrews, and N. Bellouin, 2012: Aerosols implicated as a prime driver of twentieth-century North Atlantic climate variability. *Nature*, **484**, 228–232, <https://doi.org/10.1038/nature10946>.
- Bower, A. S., R. M. Hendry, D. E. Amrhein, and J. M. Lilly, 2013: Direct observations of formation and propagation of subpolar eddies into the subtropical North Atlantic. *Deep-Sea Res. II*, **85**, 15–41, <https://doi.org/10.1016/j.dsr2.2012.07.029>.
- Buckley, M. W., and J. Marshall, 2016: Observations, inferences, and mechanisms of Atlantic meridional overturning circulation variability: A review. *Rev. Geophys.*, **54**, 5–63, <https://doi.org/10.1002/2015RG000493>.
- Burkholder, K. C., and M. S. Lozier, 2011: Subtropical to subpolar pathways in the North Atlantic: Deductions from Lagrangian trajectories. *J. Geophys. Res.*, **116**, C07017, <https://doi.org/10.1029/2010JC006697>.
- Chafik, L., S. Hakkinen, M. H. England, J. A. Carton, S. Nigam, A. Ruiz-Barradas, A. Hannachi, and L. Miller, 2016: Global linkages originating from decadal oceanic variability in the

- subpolar North Atlantic. *Geophys. Res. Lett.*, **43**, 10909–10919, <https://doi.org/10.1002/2016GL071134>.
- Chang, P., L. Ji, and H. Li, 1997: A decadal climate variation in the tropical Atlantic Ocean from thermodynamic air–sea interactions. *Nature*, **385**, 516–518, <https://doi.org/10.1038/385516a0>.
- Clement, A., K. Bellomo, L. N. Murphy, M. A. Cane, T. Mauritzen, G. Rädel, and B. Stevens, 2015: The Atlantic multidecadal oscillation without a role for ocean circulation. *Science*, **350**, 320–324, <https://doi.org/10.1126/science.aab3980>.
- Cleveland, W. S., and C. L. Loader, 1996: Smoothing by local regression: Principles and methods. *Statistical Theory and Computational Aspects of Smoothing*, W. Härdle and M. G. Schimek, Eds., Springer, 10–49.
- Czaja, A., and C. Frankignoul, 2002: Observed impact of Atlantic SST anomalies on the North Atlantic Oscillation. *J. Climate*, **15**, 606–623, [https://doi.org/10.1175/1520-0442\(2002\)015<0606:OIOASA>2.0.CO;2](https://doi.org/10.1175/1520-0442(2002)015<0606:OIOASA>2.0.CO;2).
- , and N. Blunt, 2011: A new mechanism for ocean–atmosphere coupling in midlatitudes. *Quart. J. Roy. Meteor. Soc.*, **137**, 1095–1101, <https://doi.org/10.1002/qj.814>.
- , P. van der Vaart, and J. Marshall, 2002: A diagnostic study of the role of remote forcing in tropical Atlantic variability. *J. Climate*, **15**, 3280–3290, [https://doi.org/10.1175/1520-0442\(2002\)015<3280:ADSOTR>2.0.CO;2](https://doi.org/10.1175/1520-0442(2002)015<3280:ADSOTR>2.0.CO;2).
- de Coëtlogon, G., C. Frankignoul, M. Bentsen, C. Delon, H. Haak, S. Masina, and A. Pardaens, 2006: Gulf Stream variability in five oceanic general circulation models. *J. Phys. Oceanogr.*, **36**, 2119–2135, <https://doi.org/10.1175/JPO2963.1>.
- Delworth, T., S. Manabe, and R. J. Stouffer, 1993: Interdecadal variations of the thermohaline circulation in a coupled ocean–atmosphere model. *J. Climate*, **6**, 1993–2011, [https://doi.org/10.1175/1520-0442\(1993\)006<1993:IVOTTC>2.0.CO;2](https://doi.org/10.1175/1520-0442(1993)006<1993:IVOTTC>2.0.CO;2).
- , F. Zeng, L. Zhang, R. Zhang, G. A. Vecchi, and X. Yang, 2017: The central role of ocean dynamics in connecting the North Atlantic Oscillation to the extratropical component of the Atlantic multidecadal oscillation. *J. Climate*, **30**, 3789–3805, <https://doi.org/10.1175/JCLI-D-16-0358.1>.
- Deser, C., and M. L. Blackmon, 1993: Surface climate variations over the North Atlantic Ocean during winter: 1900–1989. *J. Climate*, **6**, 1743–1753, [https://doi.org/10.1175/1520-0442\(1993\)006<1743:SCVOTN>2.0.CO;2](https://doi.org/10.1175/1520-0442(1993)006<1743:SCVOTN>2.0.CO;2).
- , M. A. Alexander, S.-P. Xie, and A. S. Phillips, 2010: Sea surface temperature variability: Patterns and mechanisms. *Annu. Rev. Mar. Sci.*, **2**, 115–143, <https://doi.org/10.1146/annurev-marine-120408-151453>.
- Dickson, R. R., J. Meincke, S. A. Malmberg, and L. J. Lee, 1988: The “great salinity anomaly” in the northern North Atlantic 1968–1982. *Prog. Oceanogr.*, **20**, 103–151, [https://doi.org/10.1016/0079-6611\(88\)90049-3](https://doi.org/10.1016/0079-6611(88)90049-3).
- Drews, A., and R. J. Greatbatch, 2016: Atlantic multidecadal variability in a model with an improved North Atlantic Current. *Geophys. Res. Lett.*, **43**, 8199–8206, <https://doi.org/10.1002/2016GL069815>.
- Enfield, D. B., A. M. Mestas-Núñez, and P. J. Trimble, 2001: The Atlantic multidecadal oscillation and its relation to rainfall and river flows in the continental U.S. *Geophys. Res. Lett.*, **28**, 2077–2080, <https://doi.org/10.1029/2000GL012745>.
- Frankignoul, C., G. de Coëtlogon, T. M. Joyce, and S. Dong, 2001: Gulf Stream variability and ocean–atmosphere interactions. *J. Phys. Oceanogr.*, **31**, 3516–3529, [https://doi.org/10.1175/1520-0485\(2002\)031<3516:GSVAOA>2.0.CO;2](https://doi.org/10.1175/1520-0485(2002)031<3516:GSVAOA>2.0.CO;2).
- Fuglister, F. C., 1963: Gulf Stream '60. *Prog. Oceanogr.*, **1**, 265–373, [https://doi.org/10.1016/0079-6611\(63\)90007-7](https://doi.org/10.1016/0079-6611(63)90007-7).
- Gastineau, G., and C. Frankignoul, 2015: Influence of the North Atlantic SST variability on the atmospheric circulation during the twentieth century. *J. Climate*, **28**, 1396–1416, <https://doi.org/10.1175/JCLI-D-14-00424.1>.
- Good, S. A., M. J. Marti, and N. A. Rayner, 2013: EN4: Quality controlled ocean temperature and salinity profiles and monthly objective analyses with uncertainty estimates. *J. Geophys. Res. Oceans*, **118**, 6704–6716, <https://doi.org/10.1002/2013JC009067>.
- Guan, B., and S. Nigam, 2009: Analysis of Atlantic SST variability factoring inter-basin links and the secular trend: Clarified structure of the Atlantic multidecadal oscillation. *J. Climate*, **22**, 4228–4240, <https://doi.org/10.1175/2009JCLI2921.1>.
- Gulev, S. K., M. Latif, N. Keenlyside, W. Park, and K. P. Koltermann, 2013: North Atlantic Ocean control on surface heat flux on multidecadal timescales. *Nature*, **499**, 464–467, <https://doi.org/10.1038/nature12268>.
- Hameed, S., and S. Piontkovski, 2004: The dominant influence of the Icelandic low on the position of the Gulf Stream north wall. *Geophys. Res. Lett.*, **31**, L09303, <https://doi.org/10.1029/2004GL019561>.
- Han, G., N. Chen, and Z. Ma, 2014: Is there a north–south phase shift in the surface Labrador Current on the interannual-to-decadal scale? *J. Geophys. Res. Oceans*, **119**, 276–287, <https://doi.org/10.1002/2013JC009102>.
- Hátún, H., A.-B. Sandø, H. Drange, B. Hansen, and H. Valdimarsson, 2005: Influence of the Atlantic subpolar gyre on the thermohaline circulation. *Science*, **309**, 1841–1844, <https://doi.org/10.1126/science.1114777>.
- Hoskins, B. J., and P. J. Valdes, 1990: On the existence of stormtracks. *J. Atmos. Sci.*, **47**, 1854–1864, [https://doi.org/10.1175/1520-0469\(1990\)047<1854:OTEOST>2.0.CO;2](https://doi.org/10.1175/1520-0469(1990)047<1854:OTEOST>2.0.CO;2).
- Hurrell, J. W., 1995: Decadal trends in the North Atlantic Oscillation: Regional temperatures and precipitation. *Science*, **269**, 676–679, <https://doi.org/10.1126/science.269.5224.676>.
- Ishii, M., and M. Kimoto, 2009: Reevaluation of historical ocean heat content variations with time-varying XBT and MBT depth bias corrections. *J. Oceanogr.*, **65**, 287–299, <https://doi.org/10.1007/s10872-009-0027-7>.
- Joyce, T. M., and R. Zhang, 2010: On the path of the Gulf Stream and the Atlantic meridional circulation. *J. Climate*, **23**, 3146–3154, <https://doi.org/10.1175/2010JCLI3310.1>.
- , C. Deser, and M. Spall, 2000: The relation between decadal variability of subtropical mode water and the North Atlantic Oscillation. *J. Climate*, **13**, 2550–2569, [https://doi.org/10.1175/1520-0442\(2000\)013<2550:TRBDVO>2.0.CO;2](https://doi.org/10.1175/1520-0442(2000)013<2550:TRBDVO>2.0.CO;2).
- Kalnay, E., and Coauthors, 1996: The NCEP/NCAR 40-Year Reanalysis Project. *Bull. Amer. Meteor. Soc.*, **77**, 437–471, [https://doi.org/10.1175/1520-0477\(1996\)077<0437:TNYRP>2.0.CO;2](https://doi.org/10.1175/1520-0477(1996)077<0437:TNYRP>2.0.CO;2).
- Kavvada, A., 2014: Atlantic multidecadal variability: Surface and subsurface thermohaline structure and hydroclimate impacts. Ph.D. thesis, University of Maryland, 152 pp.
- , A. Ruiz-Barradas, and S. Nigam, 2013: AMO’s structure and climate footprint in observations and IPCC AR5 climate simulations. *Climate Dyn.*, **41**, 1345–1364, <https://doi.org/10.1007/s00382-013-1712-1>.
- Kerr, R. A., 2000: A North Atlantic climate pacemaker for the centuries. *Science*, **288**, 1984–1985, <https://doi.org/10.1126/science.288.5473.1984>.
- Knight, J. R., R. J. Allan, C. K. Folland, M. Vellinga, and M. E. Mann, 2005: A signature of persistent natural thermohaline circulation cycles in observed climate. *Geophys. Res. Lett.*, **32**, L20708, <https://doi.org/10.1029/2005GL024233>.

- Langehaug, H. R., I. Medhaug, T. Eldevik, and O. H. Ottera, 2012: Arctic/Atlantic exchanges via the subpolar gyre. *J. Climate*, **25**, 2421–2439, <https://doi.org/10.1175/JCLI-D-11-00085.1>.
- Latif, M., and N. S. Keenlyside, 2011: A perspective on decadal climate variability and predictability. *Deep-Sea Res. II*, **58**, 1880–1894, <https://doi.org/10.1016/j.dsr2.2010.10.066>.
- Levitus, S., J. Antonov, and T. Boyer, 2009: Global ocean heat content 1955–2007 in light of recently revealed instrumentation problems. *Geophys. Res. Lett.*, **36**, L07608, <https://doi.org/10.1029/2008GL037155>.
- Marshall, J., and Coauthors, 2001: North Atlantic climate variability: Phenomena, impacts and mechanisms. *Int. J. Climatol.*, **21**, 1863–1898, <https://doi.org/10.1002/joc.693>.
- McCarthy, G. D., I. D. Haigh, J. J.-M. Hirschi, J. P. Grist, and D. A. Smeed, 2015: Ocean impact on decadal Atlantic climate variability revealed by sea-level observations. *Nature*, **521**, 508–510, <https://doi.org/10.1038/nature14491>.
- Nigam, S., 2003: Teleconnections. *Encyclopedia of Atmospheric Sciences*, 1st ed., J. R. Holton, J. A. Pyle, and J. A. Curry, Eds., Academic Press, 2243–2269.
- , and S. C. Chan, 2009: On the summertime strengthening of the Northern Hemisphere Pacific sea level pressure anticyclone. *J. Climate*, **22**, 1174–1192, <https://doi.org/10.1175/2008JCLI2322.1>.
- , and B. Guan, 2011: Atlantic tropical cyclones in the twentieth century: Natural variability and secular change in cyclone count. *Climate Dyn.*, **36**, 2279–2293, <https://doi.org/10.1007/s00382-010-0908-x>.
- , and S. Baxter, 2015: Teleconnections. *Encyclopedia of Atmospheric Sciences*, 2nd ed., G. North, F. Zhang, and J. Pyle, Eds., Academic Press, 90–109.
- , and A. Ruiz-Barradas, 2016: Key role of the Atlantic multidecadal oscillation in twentieth century drought and wet periods over the US Great Plains and the Sahel. *Dynamics and Predictability of Large-Scale High-Impact Weather and Climate Events*, J. Li et al., Eds., Cambridge University Press, 255–270.
- , B. Guan, and A. Ruiz-Barradas, 2011: Key role of the Atlantic multidecadal oscillation in 20th century drought and wet periods over the Great Plains. *Geophys. Res. Lett.*, **38**, L16713, <https://doi.org/10.1029/2011GL048650>.
- O'Reilly, C. H., M. Huber, T. Woollings, and L. Zanna, 2016: The signature of low-frequency oceanic forcing in the Atlantic Multidecadal Oscillation. *Geophys. Res. Lett.*, **43**, 2810–2818, doi:10.1002/2016GL067925.
- Peings, Y., and G. Magnusdottir, 2016: Wintertime atmospheric response to Atlantic multidecadal variability: Effect of stratospheric representation and ocean–atmosphere coupling. *Climate Dyn.*, **47**, 1029–1047, <https://doi.org/10.1007/s00382-015-2887-4>.
- Pérez-Hernández, M. D., and T. M. Joyce, 2014: Two modes of Gulf Stream variability revealed in the last two decades of satellite altimeter data. *J. Phys. Oceanogr.*, **44**, 149–163, <https://doi.org/10.1175/JPO-D-13-0136.1>.
- Quenouille, M. H., 1952: *Associated Measurements*. Academic Press, 242 pp.
- Rayner, N. A., D. E. Parker, E. B. Horton, C. K. Folland, L. V. Alexander, D. P. Rowell, E. C. Kent, and A. Kaplan, 2003: Global analyses of sea surface temperature, sea ice, and night marine air temperature since the late nineteenth century. *J. Geophys. Res.*, **108**, 4407, <https://doi.org/10.1029/2002JD002670>.
- Reintges, A., M. Latif, and W. Park, 2017: Sub-decadal North Atlantic Oscillation variability in observations and the Kiel Climate Model. *Climate Dyn.*, **48**, 3475–3487, <https://doi.org/10.1007/s00382-016-3279-0>.
- Rodwell, M. J., and C. K. Folland, 2002: Atlantic air–sea interaction and seasonal predictability. *Quart. J. Roy. Meteor. Soc.*, **128**, 1413–1443, <https://doi.org/10.1002/qj.200212858302>.
- Ruiz-Barradas, A., J. A. Carton, and S. Nigam, 2000: Structure of interannual-to-decadal climate variability in the tropical Atlantic sector. *J. Climate*, **13**, 3285–3297, [https://doi.org/10.1175/1520-0442\(2000\)013<3285:SOITDC>2.0.CO;2](https://doi.org/10.1175/1520-0442(2000)013<3285:SOITDC>2.0.CO;2).
- Sanchez-Franks, A., S. Hameed, and R. A. Wilson, 2016: The Icelandic low as a predictor of the Gulf Stream north wall position. *J. Phys. Oceanogr.*, **46**, 817–826, <https://doi.org/10.1175/JPO-D-14-0244.1>.
- Slonosky, V. C., L. A. Mysak, and J. Derome, 1997: Linking Arctic sea-ice and atmospheric circulation anomalies on interannual and decadal timescales. *Atmos.–Ocean*, **35**, 333–366, <https://doi.org/10.1080/07055900.1997.9649596>.
- Sutton, R., W. A. Norton, and S. P. Jewson, 2000: The North Atlantic Oscillation—What role for the ocean? *Atmos. Sci. Lett.*, **1**, 89–100, <https://doi.org/10.1006/asle.2000.0021>.
- Tanimoto, Y., and S.-P. Xie, 1999: Ocean–atmosphere variability over the pan-Atlantic basin. *J. Meteor. Soc. Japan*, **77**, 31–46, [https://doi.org/10.2151/jmsj1965.77.1\\_31](https://doi.org/10.2151/jmsj1965.77.1_31).
- Taylor, A. H., and J. A. Stephens, 1998: The North Atlantic Oscillation and the latitude of the Gulf Stream. *Tellus*, **50A**, 134–142, <https://doi.org/10.3402/tellusa.v50i1.14517>.
- Visbeck, M., E. P. Chassignet, R. G. Curr, T. L. Delworth, R. R. Dickson, G. Krahnemann, 2003: The ocean's response to North Atlantic Oscillation variability. *The North Atlantic Oscillation: Climatic Significance and Environmental Impact*, *Geophys. Monogr.*, Vol. 134, Amer. Geophys. Union, 113–145.
- Zhang, R., 2008: Coherent surface–subsurface fingerprint of the Atlantic meridional overturning circulation. *Geophys. Res. Lett.*, **35**, L20705, <https://doi.org/10.1029/2008GL035463>.
- , 2017: On the persistence and coherence of subpolar sea surface temperature and salinity anomalies associated with the Atlantic multidecadal variability. *Geophys. Res. Lett.*, **44**, 7865–7875, <https://doi.org/10.1002/2017GL074342>.
- , and Coauthors, 2013: Have aerosols caused the observed Atlantic multidecadal variability? *J. Atmos. Sci.*, **70**, 1135–1144, <https://doi.org/10.1175/JAS-D-12-0331.1>.
- , R. Sutton, G. Danabasoglu, T. L. Delworth, W. M. Kim, J. Robson, and S. G. Yeager, 2016: Comment on “The Atlantic multidecadal oscillation without a role for ocean circulation.” *Science*, **352**, 1527, <https://doi.org/10.1126/science.aaf1660>.